

UV and (V)UV irradiation of sitagliptin in ultrapure water and WWTP effluent: Kinetics, transformation products and degradation pathway

Dániel Krakkó^{a,b}, Ádám Illés^c, Attila Domján^d, Attila Demeter^c, Sándor Dóbé^c, Gyula Záray^{a,b,e,*}

^a Laboratory for Environmental Chemistry and Bioanalytics, Institute of Chemistry, ELTE - Eötvös Loránd University, H-1117, Budapest, Pázmány Péter sétány 1/A, Hungary

^b Cooperative Research Center for Environmental Sciences, ELTE - Eötvös Loránd University, H-1117, Budapest, Pázmány Péter sétány 1/A, Hungary

^c Renewable Energy Research Group, Institute of Materials and Environmental Chemistry, Research Centre for Natural Sciences, H-1117, Budapest, Magyar tudósok körútja 2, Hungary

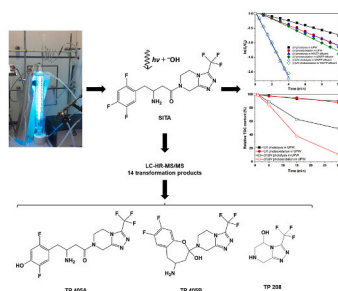
^d NMR Research Laboratory, Research Centre for Natural Sciences, H-1117, Budapest, Magyar tudósok körútja 2, Hungary

^e Environmental Chemistry Research Group, Institute of Aquatic Ecology, Centre for Ecological Research, H-1113, Budapest, Karolina út 29-31, Hungary

HIGHLIGHTS

- Degradation of SITA was examined under UV and (V)UV light.
- (V)UV irradiation was effective in degrading SITA in spiked WWTP effluent.
- 14 transformation products were identified with structure proposals.
- Some recalcitrant transformation products could not be completely eliminated.

GRAPHICAL ABSTRACT



ARTICLE INFO

Handling Editor: Jun Huang

Keywords:

Antidiabetic drug
AOP
Transformation products
UV-C
VUV/UV
Wastewater treatment

ABSTRACT

Sitagliptin (SITA) is an antidiabetic drug consumed worldwide in high quantities. Because of the low removal rate of this compound in conventional wastewater treatment plants (WWTPs), it enters receiving surface waters with the discharged WWTP effluents. SITA can be detected up to $\mu\text{g/L}$ concentration in rivers. In this study, UV (254 nm) and (V)UV (185 nm + 254 nm) irradiation was applied in laboratory scale to degrade SITA. The effect of three parameters was evaluated on the degradation rate, namely i) the efficiency in UV and (V)UV irradiation, ii) the presence or absence of dissolved oxygen, iii) the matrix effect of WWTP effluent. Degradation rate of SITA was largely increased by (V)UV irradiation, and decreased in WWTP effluent as expected. The presence of dissolved oxygen increased the degradation rate only in UV experiments and did not have a considerable effect in (V)UV experiments. In total, 14 transformation products (TPs) were identified (twelve new); their structures were proposed based on high-resolution mass spectrometry and nuclear magnetic resonance spectroscopy analyses. The most characteristic reaction steps of the degradation of SITA involved nucleophilic aromatic photo-substitution whereas hydroxide ions acted as attacking nucleophiles and replaced F atoms of the phenyl moiety by hydroxide groups, in agreement with the increase in photolysis rate with increasing pH. The photochemical

* Corresponding author. Laboratory for Environmental Chemistry and Bioanalytics, Institute of Chemistry, ELTE - Eötvös Loránd University, H-1117, Budapest, Pázmány Péter sétány 1/A, Hungary.

E-mail address: zaray.gyula@ecolres.hu (G. Záray).

<https://doi.org/10.1016/j.chemosphere.2021.132393>

Received 28 May 2021; Received in revised form 5 September 2021; Accepted 26 September 2021

Available online 30 September 2021

0045-6535/© 2021 The Authors.

Published by Elsevier Ltd.

This is an open access article under the CC BY-NC-ND license

(<http://creativecommons.org/licenses/by-nc-nd/4.0/>).

degradation pathway of SITA was also interpreted. Kinetic profiles revealed TP 421, TP 208 and TP 192 to be the most recalcitrant TPs.

1. Introduction

There are about 4000 active pharmaceutical ingredients (APIs) used as prescription medicines, over-the-counter therapeutic drugs and veterinary drugs around the world (OECD, 2019). Their consumption still increases on an annual basis. Pharmaceuticals administered to humans and animals are not completely metabolized and a substantial amount of them leave the body as active substances in urine or feces. Excretion in unchanged form can reach >90% in urine (Lienert et al., 2007). After excretion, pharmaceuticals entering the communal sewer system reach wastewater treatment plants (WWTPs). Since conventional wastewater treatment has been designed for the removal of gross organic and inorganic matter as well as suspended solids and pathogens, WWTPs are often inefficient in removing pollutants that are usually present in $\mu\text{g/L}$ concentrations (Comber et al., 2018). Thus, WWTPs are generally recognized as the major source for pharmaceuticals entering the aquatic environment via discharge of effluents into rivers (Ramirez et al., 2009). However, other non-wastewater emission sources of APIs into the environment should also be considered such as direct disposal of drugs into the sewer system or drugs thrown away with household waste (Bu et al., 2016). The presence of APIs in the aquatic environment has raised major concerns, as their effect on different organisms is not fully understood. Moreover, it is hard to predict the possible cocktail effects that these compounds can pose together to the aquatic ecosystem (European Commission, 2019). Adverse effect of APIs that have been documented include organ damage and reduced hatching success in fish as well as endocrine disrupting effects (Crago et al., 2016; Mathias et al., 2018; Xia et al., 2017), behavior changes, reduced growth and reproduction in invertebrates (Jonsson et al., 2014), reproduction toxicity in frogs (Gyllenhammar et al., 2009), etc. Some APIs can also reach riverbank filtrates and enter the drinking water supply systems (Kondor et al., 2021).

To reduce environmental concentrations of micropollutants, implementation of new technologies for post-treatment of wastewater is required. Advanced oxidation processes (AOPs) are widely studied and can provide sufficient attenuation of organic micropollutants. AOPs involve the *in situ* generation of highly potent chemical oxidants, such as hydroxyl radicals (Bolton et al., 2001). Main types include ozone based and UV-based AOPs as well as catalytic and electrochemical processes (Brillas, 2020; Miklos et al., 2018; Wardenier et al., 2019). Disinfection of biologically treated WWTP effluent is often achieved by UV irradiation prior to discharge. In this case, application of low-pressure mercury germicidal lamps, mainly emitting light at 254 nm, is preferred. Although some compounds such as diclofenac can effectively be degraded by this light (Krakkó et al., 2019a; Roscher et al., 2016), it has limited efficiency for most APIs. New types of low-pressure mercury or excimer lamps that have high and stable photon emission in the vacuum UV (VUV) range have the potential to replace conventional germicide lamps because high energy VUV photons can directly generate hydroxyl radicals in large concentration from water molecules, providing faster and more effective attenuation of a wide variety of emerging pollutants.

Diabetes mellitus or diabetes is a chronic disease that has been considered as one of the major health problems of the century and one of the leading causes of death worldwide. Each year, millions of people die as a direct consequence of diabetes or because of elevated risks of cardiovascular and other diseases (World Health Organization, 2016). The number of adults living with diabetes increased from 108 million in 1980 to 422 million in 2014 (World Health Organization, 2016). Sitagliptin (SITA) is the first member of the drug class of gliptins. It is an orally administered selective inhibitor of the enzyme dipeptidyl peptidase-4, and it is used for the treatment of type 2 diabetes (Gallwitz,

2007). It was approved by the Food and Drug Administration of the United States in October 2006 as monotherapy and as add-on therapy together with metformin or thiazolidinediones (Drucker et al., 2007; Yuzbasioglu et al., 2018). In March 2007, it was also approved by the European Union (Yuzbasioglu et al., 2018). The action of SITA is mediated by increasing levels of glucagon-like peptide-1 hormones and gastric inhibitory polypeptide (Gallwitz, 2007). SITA has a bioavailability of 87% and a low and reversible binding to plasma proteins in approximately 38% (Herman et al., 2007). About 79% of the administered dose is excreted in unchanged form in urine (Herman et al., 2007). SITA was detected in WWTP influents and effluents up to several $\mu\text{g/L}$ concentrations (Herman et al., 2007; Ibáñez et al., 2017; Krakkó et al., 2019b; Martín et al., 2012) and in river water and sediment in low ng/L (Boulard et al., 2020; Krakkó et al., 2019b).

There is scarce information about the degradation of SITA in the literature. Although some studies focused on its chemical stability in stressed conditions e.g., high temperature, acidic and basic pH or oxidation in presence of H_2O_2 , (Gumieniczek et al., 2019; Salim et al., 2014; Sonune and Mone, 2013; Vishnuvardhan et al., 2014), to the best of our knowledge, it was studied in wastewater in three cases. Henning et al. investigated the biological transformation of SITA in pilot- and full-scale conventional activated sludge and moving bed biofilm reactors (Henning et al., 2019). In these experiments, removals of 46% and 62%, respectively, could be achieved. They identified nine transformation products (TPs) and eight out of nine TPs could be detected in the effluents (Henning et al., 2019). More recently, Hermes et al. investigated the ozonation of SITA in lab- and pilot-scale experiments in pure water and WWTP effluent (Hermes et al., 2018). They detected 32 possible TPs, and chemical structure was proposed in nine cases. All TPs could be detected in spiked WWTP effluent in lab-scale experiment. Six TPs could also be detected in pilot-scale experiments, and it was concluded that two out of these six TPs could not be removed by ozonation under the applied circumstances. More recently, Krakkó et al. applied pilot-scale (V)UV/O₃ technology and determined the removal of SITA and other micropollutants in WWTP effluent (Krakkó et al., 2021). In that study, SITA showed the lowest removal efficiency (41–46%) among the 7 target compounds.

To the best of our knowledge, the degradation of SITA was not yet studied in detail under UV light. The aim of this study was to investigate the effect of UV and (V)UV radiation on the degradation of SITA in both ultrapure water (UPW) and WWTP effluent, paying special attention to determine reaction kinetics, identify TPs and their structures, and propose degradation pathways.

2. Materials and methods

2.1. Chemicals and reagents

Analytical standard of sitagliptin phosphate was purchased from Sigma-Aldrich Ltd. (Budapest, Hungary). 2-Fluorophenethylamine was synthesized in our institute. Acetonitrile, methanol and formic acid (99% by weight) of LC-MS grade and 2 M hydrochloric acid were obtained from VWR International Ltd (Debrecen, Hungary). Acetic acid (96% by weight) was purchased from Merck (Merck KGaA, Darmstadt, Germany). UPW (resistivity of 18.2 M Ω cm) was acquired from an ELGA Purelab Option-R7 unit (ELGA LabWater/VWS Ltd., High Wycombe, UK).

2.2. Wastewater sampling

Biologically treated WWTP effluent was acquired from the WWTP of

Kiskunlacháza, Hungary (GPS coordinates: 47°10'38.3"N, 19°01'30.3"E). This medium-sized WWTP treats 800–1000 m³ wastewater daily. Samples were stored at 4 °C and used for experiments without dilution. Typical physico-chemical parameters of the WWTP effluent as well as the concentration of inorganic ions can be found in Table S1-2 in Supplementary Materials.

2.3. Experimental procedure

All irradiation experiments were carried out in a batch photoreactor with a liquid volume of 650 mL. UPW and WWTP effluent were spiked with SITA to either 5×10^{-6} M (kinetic measurements and identification of degradation products) or 5×10^{-5} M (determination of total organic carbon content). Two types of low-pressure mercury lamps were used; a conventional germicidal lamp ("UV lamp") and a modified version of it with a substantial vacuum UV output at 185 nm besides the dominant radiation at 254 nm ("VUV lamp"), both acquired from LightTech Ltd (Dunakeszi, Hungary). Both lamps had a length of 360 mm, the diameter of their inner quartz tube was 15 mm. The lamps were centrally placed in the photoreactor inside a Suprasil® quartz jacket with a diameter of 45 mm. The photon fluxes entering the reaction mixtures were 5.4×10^{-8} molphoton cm⁻² s⁻¹ and 7.6×10^{-8} molphoton cm⁻² s⁻¹ at 254 nm for the UV lamp and (V)UV lamp, respectively, while the photon flux of the (V)UV lamp at 185 nm was 4.6×10^{-9} molphoton cm⁻² s⁻¹. The photon fluxes have been estimated by the geometries and the 185 and 254 nm output powers of the lamps provided by the manufacturer. The distance between the surface of the quartz sleeve of the lamp and the liquid layer of the photoreactor was 15 mm, the distance between the surface of the quartz sleeve and the internal surface of the photoreactor was 24 mm. Temperature of the solution in the reactor and the cooling gas inside the Suprasil® quartz jacket were measured with Chromel-Alumel thermocouples and were between 20 and 30 °C. Photolysis experiments were carried out in the absence of dissolved oxygen achieved by continuous argon (99.996% purity) purging with a flow rate of 500 mL/min. The solution was purged with oxygen (99.95% purity) with a flow rate of 990 mL/min (additionally, ozone was produced in (V)UV photooxidation experiments). Lamps were cooled with nitrogen (99.996% purity) at 800 mL/min. All experiments were preceded by 10 min argon purging. Samples of 1 mL or 5 mL were taken at pre-determined intervals with a syringe through a plastic tube immersed into the solution. WWTP effluent samples taken for liquid chromatographic measurements were filtered through polytetrafluoroethylene syringe filters of 0.45 µm pore size. Samples of 50 mL were taken for the identification of degradation products after irradiation was stopped. Kinetic parameters were calculated based on results of three parallel experiments and two sigma limits were used for error calculation.

2.4. Analytical methods

Concentration of SITA was determined by a model 1200 high-performance liquid chromatograph from Agilent Technologies (Santa Clara, USA) equipped with binary pump, vacuum degasser, autosampler, column thermostat and variable wavelength detector. Chromatographic separation was achieved on a Phenomenex Luna 5u C18 100A (250 × 4.6 mm, 5 µm particle size) column equipped with a Phenomenex SecurityGuard C18 (4 × 3.0 mm) precolumn. The chromatographic column was kept at 40 °C. Measurements were carried out with isocratic elution of 0.1% (v/v) acetic acid in UPW:acetonitrile 85:15 (v/v) as the mobile phase at a flowrate of 1.5 mL/min. Detection wavelength was 270 nm and injection volume was 100 µL.

For the identification of degradation products, a Bruker Elute ultrahigh performance liquid chromatograph coupled to a Bruker Compact quadrupole time-of-flight mass spectrometer (Bruker Daltonik GmbH, Bremen, Germany) was used. Samples of 50 mL were preconcentrated by solid-phase extraction prior to analyses. Detailed information on the preconcentration procedure, operating conditions and chromatographic

separation can be found elsewhere (Krakkó et al., 2019a).

Nuclear magnetic resonance (NMR) spectroscopy was applied for the structural identification of TP 405B. The ¹H, ¹³C, and ¹⁹F NMR spectra were recorded on Varian NMR System 600. The structure determination was based on one- (¹H, ¹³C, ¹⁹F NMR) and two-dimensional (¹H-¹³C-gHSQCAD, ¹H-¹³C-gHMBCAD, ¹H-zqTOCSY, ¹H-NOESY) NMR experiments. Chemical shifts were expressed in parts per million (δ). The ¹H and ¹³C chemical shifts were referenced to the residual solvent signals; for ¹⁹F chemical shifts, CCl₃ internal standard was used. Coupling constants (J) were reported in hertz (Hz). Splitting patterns were designated as s (singlet), bs (broad singlet), d (doublet), t (triplet), q (quartet), and m (multiplet).

Total organic carbon (TOC) content was determined as non-purgeable organic carbon by a Multi N/C 2100S TC-TN analyzer (Analytik Jena, Jena, Germany) with an injection volume of 500 µL. Oven of the equipment was heated to 800 °C, the flowrate of oxygen (99.999% purity) was 160 mL/min. Samples were acidified with 2 M hydrochloric acid prior to analysis.

The IR spectra of SITA and the isolated TP 405B primary intermediate were recorded on a Varian 2000 FTIR Scimitar Series spectrometer (Varian Inc., USA) fitted with a single reflection diamond ATR accessory (Specac Ltd., UK).

3. Results and discussion

3.1. Removal kinetics of sitagliptin under different conditions

Three parameters were evaluated based on their effect on the degradation rate of SITA in batch-scale experiments (Fig. 1). i) Dissolved oxygen was either purged out from solutions in the batch reactor with argon (photolysis), or continuous oxygen purging was applied during irradiations (photooxidation). ii) The effect of high energy vacuum ultraviolet (VUV) photons was evaluated by using either a conventional low-pressure mercury lamp emitting photons mainly at 254 nm (referred to as UV irradiation in the text) or another low-pressure mercury lamp of identical dimensions with a substantial photon emission at 185 nm besides 254 nm (referred to as (V)UV irradiation in the text). iii) The matrix effect of real WWTP effluent was compared to experiments conducted in spiked UPW (Fig. 1).

Degradation of SITA followed pseudo-first order kinetics in all cases. Half-lives and pseudo-first order rate constants were calculated (Table 1). The effect of oxygen on the degradation rate of SITA was found to be significant only in UV irradiation. The faster degradation of SITA in (V)UV irradiation compared to UV irradiation (Fig. 1) can be explained by the formation of highly reactive species (Eqs. (1)–(5)). In case of (V)UV irradiation, VUV photons with wavelength of 185 nm are predominantly absorbed by water molecules, generating hydroxyl radicals ([•]OH) in high concentration according to Eqs. (1) and (2) (Xie et al., 2018). Other reactive oxidative species are formed in subsequent reactions (Eqs. (3)–(5)) (Xie et al., 2018). The contribution of HO₂[•] and O₂^{•-} from Eqs. (3)–(5) are probably negligible compared to that of [•]OH in case of (V)UV irradiation (Xie et al., 2018). This could explain the similarities between the degradation kinetics for (V)UV photolysis and photooxidation. Moreover, the increased degradation rate during UV photooxidation compared to UV photolysis in UPW and in WWTP effluent can be explained by the photosensitized generation of singlet oxygen, O₂(¹Δ), by the triplet excited SITA that can oxidize ground state SITA molecules. In absence of oxygen, triplet related processes can be observed on the microsecond timescale using laser flash photolysis – transient absorption technique. However, due to their lower reactivity and fast scavenging of oxygenates HO₂[•], O₂^{•-}, and O₂(¹Δ) by O₂, the reaction accelerator effect of singlet oxygen is of minor importance when (V)UV irradiation is applied (Kutschera et al., 2009; Zoschke et al., 2014).



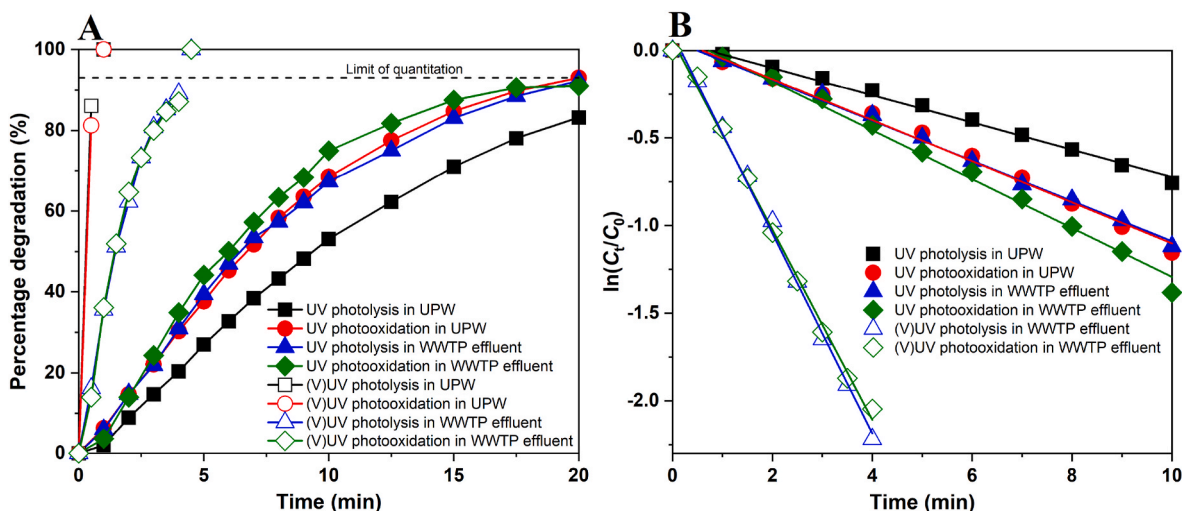


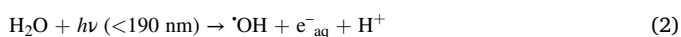
Fig. 1. Percentage degradation of sitagliptin (A) and linear regressions (B) as a function of irradiation time under different experimental conditions.

Table 1

Kinetic parameters for UV and (V)UV degradation of sitagliptin.

	UPW			
	UV irradiation		(V)UV irradiation	
	Photolysis	Photooxidation	Photolysis	Photooxidation
$t_{1/2}$ (s)	533.19 ± 32.81	355.46 ± 23.70	n.c.	n.c.
k (10^{-3} s $^{-1}$)	1.30 ± 0.08	1.95 ± 0.13	n.c.	n.c.
	WWTP effluent			
	UV irradiation		(V)UV irradiation	
	Photolysis	Photooxidation	Photolysis	Photooxidation
$t_{1/2}$ (s)	362.90 ± 17.48	298.77 ± 20.61	72.96 ± 3.53	76.76 ± 3.57
k (10^{-3} s $^{-1}$)	1.91 ± 0.09	2.32 ± 0.16	9.50 ± 0.46	9.03 ± 0.42

Abbreviations: k = pseudo-first order rate constant; n.c. = not calculated; $t_{1/2}$ = half-life; UPW = ultrapure water; WWTP = wastewater treatment plant.



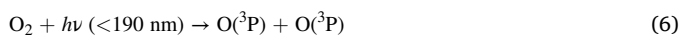
In general, faster depletion of the target compounds could be achieved by (V)UV irradiation compared to UV irradiation as it is shown in the literature (Kim et al., 2015; Krakkó et al., 2019a). This was also the case for SITA (Fig. 1). Degradation of SITA by UV irradiation in UPW was slow (>20 min), and comparable to that of carbamazepine under identical experimental conditions ($(1.31 \pm 0.12) \times 10^{-3} \text{ s}^{-1}$ and $(1.84 \pm 0.15) \times 10^{-3} \text{ s}^{-1}$ for UV photolysis and photooxidation, respectively) (Krakkó et al., 2019a). On the contrary, in (V)UV irradiation, SITA degraded within 1 min. Because of the rapid degradation, kinetic parameters could not be calculated properly in this case.

Interestingly, SITA degraded faster in WWTP effluent than in UPW in UV experiments when the pH of the solutions was not adjusted. Hermes et al. reported that SITA showed pH-dependent removal kinetics during ozonation (Hermes et al., 2020). To explain the faster degradation of SITA in WWTP effluent compared to UPW during UV irradiation, the pH dependency of SITA was studied and a clear change in degradation rate was observed (Fig. S1A-B). The rate constant of the consumption

reaction of SITA increased with increasing pH for both UV photolysis and photooxidation (Fig. S1A-B). The UV absorption spectrum of SITA around 254 nm did not show pH dependency (Fig. S2). Instead, the reason for the faster degradation was that hydroxide ions replaced one of the F atoms attached to aromatic rings in a nucleophilic aromatic photosubstitution reaction (Wubbels et al., 2008). Experiments conducted in dark for 24 h showed that the substitution reaction did not occur in the absence of UV light. The logarithm of the concentration of hydroxide ions is directly proportional to the pH. The pH of the WWTP effluent was around 7.8 that was considerably higher than that of the SITA solution prepared in UPW (pH ~ 6.8). However, the measured pseudo-first order rate constants in UPW at pH 8 were 1.9 and 1.3 times larger than in WWTP effluent for UV photolysis and photooxidation, respectively (Table S3). This way, the matrix effect of the WWTP effluent had to be considered as a slowing effect that was counteracting the degradation rate-accelerating effect of the elevated pH. The main inorganic ion constituents of WWTP effluents such as SO_4^{2-} , NO_3^- , HCO_3^- , Na^+ , K^+ , Ca^{2+} have practically zero photon absorption at 254 nm (Duca et al., 2017). None of these ions act as a hydroxyl radical scavenger, except for HCO_3^- which scavenges a small portion (8.5%) of the total hydroxyl radical content (Duca et al., 2017). This led to the conclusion that although the elevated pH of the WWTP effluent increased the degradation rate of SITA, the organic constituents counteracted and slowed it by acting as photon and/or hydroxyl radical scavengers.

Depletion of SITA by (V)UV irradiation in WWTP effluent was slower than in UPW (Table 1). In this case, SITA was depleted within 4 min in WWTP effluent compared to almost complete depletion within 1 min in UPW (Fig. 1).

The decrease of TOC content was also monitored during each experiment. Because of the small TOC content of $5 \times 10^{-6} \text{ M}$ SITA solution in UPW, these experiments were conducted with samples containing SITA in $5 \times 10^{-5} \text{ M}$ concentration. Higher mineralization of SITA by (V)UV photolysis and photooxidation compared to UV irradiation indicated that hydroxyl radicals (Eqs. (1) and (2)) played an important role in the mineralization. Although significant differences in reaction kinetics could not be observed between (V)UV photolysis and photooxidation, substantially higher mineralization was observed for (V)UV photooxidation compared to (V)UV photolysis (Fig. S3A). This meant that on average 89% and 50% of the TOC content was depleted within 30 min irradiation time (Fig. S3A). This could be explained by the formation of ozone from oxygen via reactions Eqs. (6) and (7) (Bu et al., 2016). Ozone as well as $\text{O}(^3\text{P})$ (Eq. (6)) are strong oxidizing agents that, similarly to hydroxyl radicals, can effectively mineralize a wide range of organic compounds.



For spiked WWTP effluent, a small decrease of 28% could be observed (Fig. S3B). In these experiments, less than 20% of the TOC content originated from spiking the WWTP effluent with SITA and the TOC content of the WWTP effluent consisted mainly of natural organic matter. Natural organic matter has a high degree of oxidation and thus, it is less prone to further oxidation and degradation. Moreover, fluoride ions were determined in >mg/L concentration in the solutions after mineralization experiments. This also confirms the substitution of fluoride atoms in the structure of SITA during irradiation.

3.2. Identification of transformation products

A total of 14 transformation products (TPs) were identified by liquid chromatography – high resolution mass spectrometry in UPW under UV and (V)UV irradiation (Table 2). Experiments were carried out in both the presence and absence of oxygen. The TPs that were detected and identified were most probably formed in a series of photochemical reactions and were stable in the absence of light after irradiation. The further oxidized, smaller species that could have been formed specially in photooxidation experiments were probably unstable, consequently, their concentration in the solutions were not high enough to detect them with our methodology. Therefore, photolysis and photooxidation experiments are not discussed separately in this section. SITA and most TPs could be detected in both positive and negative electrospray ionization mode, but positive mode yielded higher intensities and was used for all investigations. In (V)UV experiments, only the main TPs could be detected because of the rapid degradation as discussed in Section 3.1. A comprehensive summary of all TPs can be found in Table 4.

The MS² spectrum of SITA in positive ionization mode has been discussed in several publications (Gumieniczek et al., 2019; Hermes et al., 2020; Vishnuvardhan et al., 2014). In the first step, the protonated molecule either loses NH₃ (m/z 408.13 → m/z 391.10) or splits into two parts. In the latter case, fragments containing the triazole-piperazine moiety of SITA (m/z 235.08 and m/z 193.07; see Fig. S4 for the different moieties) or the phenyl moiety (m/z 174.05) were produced depending on the place of the positive charge in the structure. Several other smaller fragments were also identified (Fig. S5).

Based on the exact mass of TP 421, it contained one more oxygen atom and two less hydrogen atoms compared to SITA. The double bond equivalent (DBE) or degree of unsaturation of TP 421 increased by one, suggesting the formation of a new π bond. The presence of m/z 174.05 in the MS² spectrum suggested that the phenyl side of the molecule was not changed (Fig. S6). Fragment ion m/z 207.05 was identified as the oxygenated form of the m/z 193.07 fragment of SITA. In another study, three isomers with the same molecular formula were proposed (Hermes et al., 2020). TP 421 of our study shows similar fragment ions to one of the isomers that was presented by Hermes et al. (TP 421b). We propose that the piperazine ring of SITA reacted with a hydroxyl radical forming this TP. The exact place of the hydroxyl radical attack could not be verified.

TP 405A appeared in the chromatogram with three different peaks. The exact mass of the protonated molecule indicated that one of the F atoms was missing and a new hydroxyl group was attached to the molecule. The MS² spectra of the three isomers were almost identical (Fig. S7). Similarly to the MS² spectrum of SITA, m/z 235.08 and m/z 193.07 were present in the spectra of TP 405A. These fragment ions, and m/z 172.06 clearly suggested that changes in the structure took place in the phenyl moiety of SITA. This was in accordance with the above-mentioned findings that hydroxide ions can replace F atom(s) in the structure by means of nucleophilic aromatic photosubstitution. All of the identified TPs in this study were detected in UV experiments. In the case of TP 405A, the loss of F atoms by direct photolysis was not possible

because the average bond energy of a C–F bond is ~485 kJ/mol while the energy of a UV photon with wavelength of 254 nm is ~469 kJ/mol. Nucleophilic aromatic photosubstitution was further confirmed by irradiating 2-fluorophenethylamine under identical circumstances. The formation of 2-hydroxyphenethylamine from 2-fluorophenethylamine was confirmed by mass spectrometry (Fig. S8).

The lowest singlet and triplet states of SITA correspond to the transition of the electron mainly inside the trifluorophenyl ring with a considerably contribution from the β-alkylamino group. This way the F atom, in the form of F[−] becomes a better leaving group in the nucleophilic attack of a hydroxide ion. Moreover, the rate of the nucleophilic aromatic substitution of the F atom is expected to increase with the number of other halogen atoms attached to the phenyl ring. According to our view, F[−] leaves together with the proton of the hydroxide ion, resulting in a phenolate anion in the corresponding ortho, meta or para position. All are immediately stabilized by proton abstraction from water, however the oxygen atom of the ortho-phenolate group may also add to the carbon atom of the carbonyl group (as can be seen for TP 405B where a new benzoxepane ring was formed). In the latter case, the resulted alcoholate will also be stabilized by proton abstraction from the solvent. TP 405B is a structural isomer of TP 405A and it was one of the most predominant TPs in both UV and (V)UV irradiations. Its MS² spectrum completely differed from that of TP 405A (Fig. S9A–B). Based solely on the MS² spectrum, a structure could not be proposed for this compound. TP 405B was extracted by HPLC on a semipreparative chromatographic column and further analyzed by IR and NMR spectroscopy. The IR spectra of SITA and TP 405B (Fig. S9C) clearly showed that the intense carbonyl stretching bands (1668 cm^{−1} and 1425 cm^{−1}, almost at the same position as for the structurally similar 1-acetyl-piperidine that has the two bands at 1640 cm^{−1} and 1440 cm^{−1}) of SITA disappeared in the spectrum of TP 405B. This meant that the carbonyl group was modified in TP 405B. Based on the acquired ¹H, ¹³C and ¹⁹F NMR spectra (Fig. S9D–H), a new ring formation was identified. The F atom in the ortho position was substituted by an O atom and a phenyl ether bond was formed between the fluorophenyl ring and the C atom in the γ position. Crosspeaks of the NOESY spectrum of TP 405B (Fig. 2) strongly indicated that the originally meta proton (C15) of the phenyl ring had a spatial proximity (less than 5 Å) with the protons connected to the C20 and C21 positions of the tetrahydropyrimidine ring, as it was expected in the case of the suggested ring formation.

TP 403A was detected with two peaks in the chromatograms. Its exact mass indicated two F displacements by hydroxide ions. Similarly to the case of TP 405A, m/z 235.08 and m/z 193.07 in the MS² spectrum indicated that the trifluoromethyl group attached to the triazole moiety of SITA was not changed (Fig. S10). Fragment ions m/z 170.06, m/z 153.05, m/z 150.06, m/z 132.05 and m/z 125.04 were all assigned to the phenyl ring of the molecule and indicated that the two F atoms were replaced on the phenyl ring.

TP 403B is a structural isomer of TP 403A, similarly to the relation of TP 405A to TP 405B. The same fragmentation pattern was observed for TP 403B as for TP 405B, but the mass-to-charge ratio of all fragment ions was lower by 1.996, corresponding to a further substitution of a F atom with a hydroxyl group (Fig. S11).

Substitution of a third F atom could also occur. However, a structure corresponding to TP 401A could not be observed, and only TP 401B could be detected. Its MS² spectrum showed a similar pattern to TP 405B and TP 403B (Fig. S12).

The protonated molecule of TP 388 had an odd nominal mass, and this indicated an even number of nitrogen atoms in the structure. Its exact mass also suggested the loss of ammonia and substitution of a F atom as discussed earlier. Based on the MS² spectrum, the triazole-piperazine moiety did not change (m/z 193.07) (Fig. S13).

TP 387 suffered a F loss and contained only five F atoms. Fragment ions m/z 235.08 and m/z 193.07 were detected in the MS² spectrum (Fig. S14). This indicated that the F loss happened on the phenyl ring.

TP 385 had a similar MS² spectrum to that of TP 387, a loss of F was

Table 2
Identified transformation products of the UV and (V)UV degradation of sitagliptin.

Name and molecular formula [M + H ⁺]	Retention time (min)	Accurate mass [M + H ⁺] (mass accuracy)	DBE [M+H] ⁺	Structure	Level ^a
SITA C ₁₆ H ₁₆ F ₆ N ₅ O	7.8	408.1255 (0.35)	9.5		1
TP 421 C ₁₆ H ₁₄ F ₆ N ₅ O ₂	11.0	422.1061 (3.5)	10.5		3
TP 405A C ₁₆ H ₁₇ F ₅ N ₅ O ₂	4.7, 5.7, 7.5	406.1302 (1.3)	9.5		3
TP 405B C ₁₆ H ₁₇ F ₅ N ₅ O ₂	7.2	406.1288 (-2.2)	9.5		2
TP 403A C ₁₆ H ₁₈ F ₄ N ₅ O ₃	2.9, 3.3	404.1337 (-0.81)	9.5		3
TP 403B C ₁₆ H ₁₈ F ₄ N ₅ O ₃	4.1	404.1345 (1.2)	9.5		3
TP 401B C ₁₆ H ₁₉ F ₃ N ₅ O ₄	2.8	402.1383 (-0.16)	9.5		3
TP 388 C ₁₆ H ₁₄ F ₅ N ₄ O ₂	12.2	389.1032 (0.15)	10.5		3

(continued on next page)

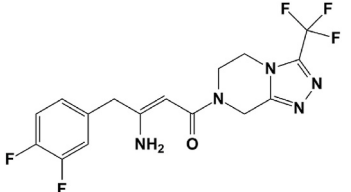
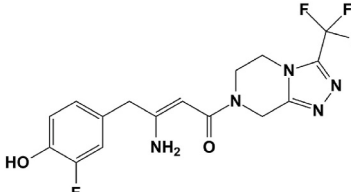
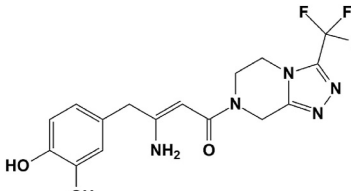
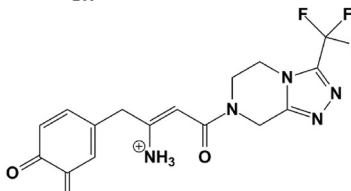
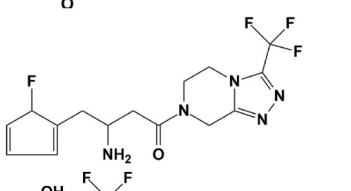


identified. Moreover, based on fragment ion m/z 152.05, a F atom was replaced by a hydroxyl group (Fig. S15).

In case of TP 383, structure proposal was mainly based on TPs 387 and 385 and the presence of fragment ion m/z 193.07 in the MS²

spectrum. Only two fragment ions were detected because this compound was present only in traces (Fig. S16).

The difference between TP 383 and TP 381 was two H atoms (Fig. S17). Taking into consideration that the piperazine-triazole moiety

Table 2 (continued)

Name and molecular formula [M + H ⁺]	Retention time (min)	Accurate mass [M + H ⁺] (mass accuracy)	DBE [M+H] ⁺	Structure	Level ^a
TP 387 C ₁₆ H ₁₅ F ₅ N ₅ O	14.1	388.1197 (1.5)	10.5		3
TP 385 C ₁₆ H ₁₆ F ₄ N ₅ O ₂	8.9	386.1241 (1.7)	10.5		3
TP 383 C ₁₆ H ₁₇ F ₃ N ₅ O ₃	1.4	384.1285 (1.8)	10.5		3
TP 381 C ₁₆ H ₁₅ F ₃ N ₅ O ₃	5.7	382.1130 (2.2)	11.5		3
TP 359 C ₁₅ H ₁₈ F ₄ N ₅ O	5.7	360.1444 (0.56)	8.5		3
TP 208 C ₆ H ₈ F ₃ N ₄ O	1.7	209.0646 (0.61)	4.5		3
TP 192 C ₆ H ₈ F ₃ N ₄	0.9	193.0694 (-0.81)	4.5		2

^a Identification confidence level in high resolution mass spectrometric analysis as proposed by Schymanski et al., (2014).

of the molecule did not change (m/z 193.07), a benzoquinone structure was proposed for TP 381.

TP 359 showed losses of two F and one C atoms. Based on its fragment ions these losses took place on the phenyl ring and the triazole-piperazine moiety was not changed (Fig. S18).

TP 208 (Fig. S19) and TP 192 (Fig. S20) were detected in all experiments. TP 192 was probably formed after photolytic cleavage of SITA. The formation of TP 192 from most of the other TPs could also be possible. This compound was previously identified in stressed acidic and basic conditions or thermal degradation (Gumieniczek et al., 2019; Salim et al., 2014; Sonune and Mone, 2013; Vishnuvardhan et al., 2014), after ozonation (Hermes et al., 2020) and biological transformation during wastewater treatment (Henning et al., 2019). TP 192 is also known as an impurity of SITA (Sonune and Mone, 2013). TP 208 was a hydroxylated product of TP 192 (Fig. S19) with similar fragment ions (m/z 191.05, m/z 138.03, m/z 108.02 and m/z 72.05). The exact

location of the hydroxyl group could not be identified.

3.3. Degradation pathway

The proposed degradation pathway of SITA (Fig. 3) is the same for photolysis and photooxidation because only the ratios of the TPs were different in those experiments. Degradation of SITA was initiated by series of nucleophilic aromatic photosubstitution reactions. In the first step, F displacement in the phenyl ring of SITA took place (TP 405A). The F atoms in all three positions on the phenyl ring may be substituted with the meta position being the least favored. Based on the reaction that followed the first F substitution, we differentiated between Routes 1A and 1B. In the former case, the first F substitution was followed by a second (TP 403A). Replacement of the third F atom in the phenyl ring was also probable (TP 401A), but such TP could not be detected in any of the experiments. In the competitive Route 1B, the ortho F substitution

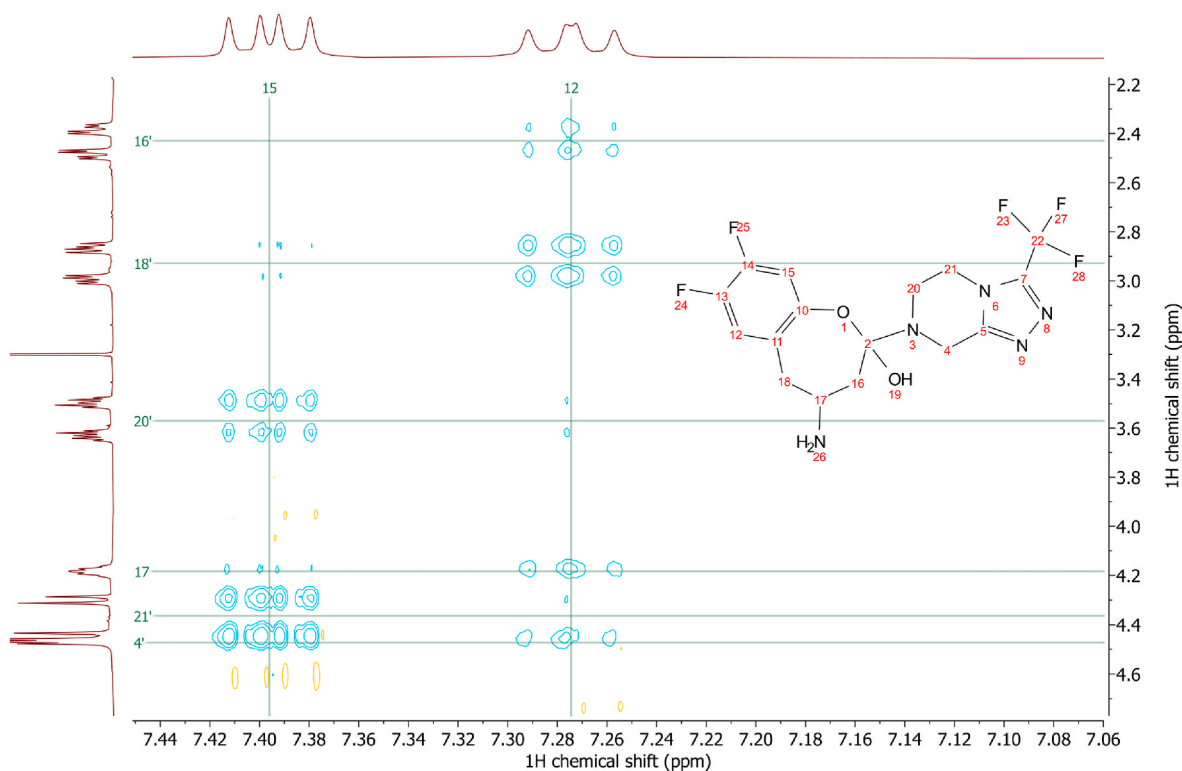


Fig. 2. The NOESY spectrum of TP 405B recorded in acetone-d₆ with contact time of 500 ms.

occurred together with a concerted intramolecular cyclization (TP 405B), resulting in a seven-membered ring (a benzoxepane derivative). Substitution of the other two F atoms in the phenyl ring of TP 405B in consequent reactions was also observed (TP 403B and TP 401B).

In Route 2, photolytic cleavage of the amide bond of SITA resulted in the formation of TP 192. Oxidation of TP 192 gave TP 208. TP 192 could be formed from all the other TPs identified in this study. When photolytic cleavage of the amide bond happens, other fragments containing the phenyl moiety are formed besides TP 192. However, these fragments could not be detected in any case which could be due to 1) high instability and fast degradation of these TPs, 2) low sensitivity and poor ionization, especially in case of a further amine loss.

The detailed mechanism for the formation of TP 387 is not known. According to our views, the alkyl amino group of SITA in excited state has a δ^+ charge, thus most probably, it may form an intramolecular complex where the ortho F is in the close proximity of the aminoalkyl group. Consequently, F⁻ may leave from the ortho position from the charge transfer conformer together with the proton of the nearby methyne (C17). In a concerted reaction, the ring can gain a proton from the neighboring methylene group (C16) and the remaining structure can stabilize as TP 387 (Route 3). Photosubstitution of the two F atoms on the phenyl ring of TP 387 was also observed (TP 385 and TP 383). Further oxidation resulted in a 1,2-benzoquinone-like structure (TP 381).

As mentioned above, in its excited state, SITA may have a conformer where the NH₂ group is in the proximity of the ortho F atom. The acidic F, when substituted by a hydroxide ion, may leave together with the NH₂ group (basic character), resulting in the structure of TP 388 (Route 4).

Route 5 consisted solely of the formation of TP 421. This TP could not be directly connected to any of the other routes but could have possibly underwent similar reactions as SITA itself.

TP 359 suffered losses of two F and one C atoms, its formation is unknown and was designated as Route 6. This TP was observed only in traces.

3.4. Kinetic profile of the transformation products

Kinetic profiles of photolysis (Fig. S21) and photooxidation (Fig. 4) experiments were very similar in each case. Degradation of SITA was primarily driven by nucleophilic aromatic substitution reactions. Routes 1A and 1B were the most dominant in case of UV irradiation in spiked UPW (Fig. 4A and Fig. S21A). In UV experiments, photolytic cleavage and the formation of TP 192 through Route 2 was more relevant in spiked WWTP effluent (Fig. 4B and Fig. S20B). In case of photolysis, all compounds were detected in spiked UPW (Fig. S21A), however, TP 401B, TP 383 and TP 381 could not be detected in spiked WWTP effluent (Fig. S21B). In photooxidation experiments, one (TP 385) and six compounds (TP 403A, TP 401B, TPs 385A, TP 383, TP 381) could not be detected in UPW and WWTP effluent, respectively (Fig. 4A and B). Only seven compounds (TP 421, TPs 405A/B, TPs 403A/B, TP 208 and TP 192) were detected in (V)UV photolysis and photooxidation (Fig. 4C–D and Fig. S21C–D). TP 421, TP 208 and TP 192 were identified as most recalcitrant TPs that could not be completely eliminated even after 60 min of (V)UV photooxidation in WWTP effluent. Overall, TP 421, TP 405A, TP 405B, TP 208 and TP 192 are the most significant TPs that were produced in the largest quantity.

Although complete abatement of all TPs of SITA could not be achieved by any of the four treatment conditions (UV photolysis, UV photooxidation, (V)UV photolysis and (V)UV photooxidation) in WWTP effluent, the sum of all peak areas was generally one order of magnitude lower for (V)UV photolysis and photooxidation compared to UV photolysis and photooxidation, respectively. Moreover, replacement of F atom to hydroxyl group increases biodegradability of SITA by bacteria. This makes (V)UV irradiation a useful method for the removal of SITA or other micropollutants from WWTP effluent.

4. Conclusions

It is well known that SITA can be detected in WWTP effluents and river water (Boulard et al., 2020; Hermes et al., 2018; Ibáñez et al.,

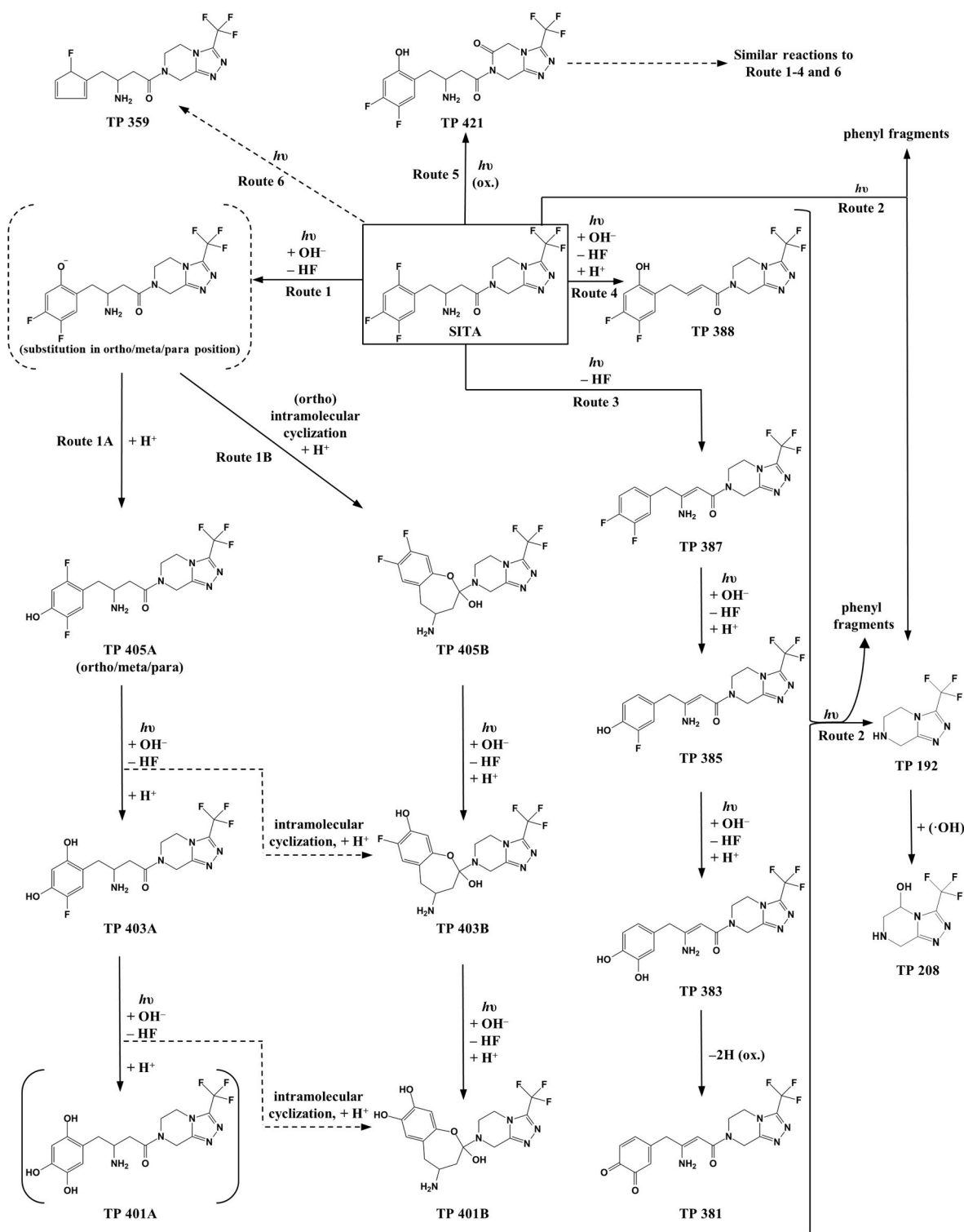


Fig. 3. Proposed degradation pathway of SITA under UV and (V)UV irradiation.

2017; Krakkó et al., 2019b; Martín et al., 2012). If UV disinfection is applied in a WWTP before discharging the effluent, degradation of this compound can be expected. Solar degradation can also play a significant role in the attenuation of SITA, although further studies are needed to prove this hypothesis. In conclusion, it is important to monitor not only the parent compound itself but its main TPs in treated and disinfected WWTP effluents and in surface water. In our study, 14 TPs were identified during conventional UV and more powerful (V)UV irradiation in both UPW and WWTP effluent in batch-scale experiments. Twelve TPs

were reported for the first time. TP 421, TP 405A, TP 405B, TP 208 and TP 192 are the most significant TPs that we propose to be monitored along with SITA in environmental samples.

Credit author statement

Dániel Krakkó; : Investigation, Writing – original draft, Visualization. Ádám Illés: Investigation, Visualization. Attila Domján: Investigation. Attila Demeter: Investigation, Writing – review & editing. Sándor Dóbcé:

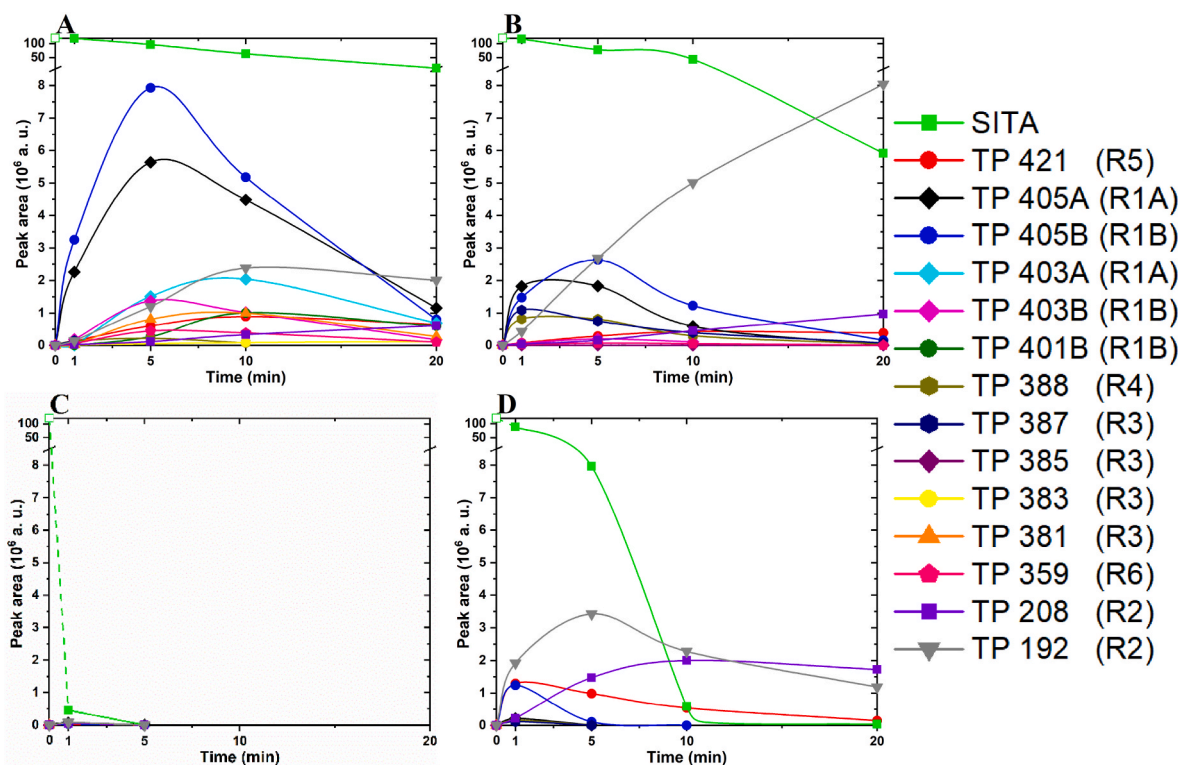


Fig. 4. Kinetic profile of sitagliptin and its 14 transformation products during UV photooxidation in UPW (A), in WWTP effluent (B), in (V)UV photooxidation in UPW (C) and in WWTP effluent (D).

Writing – review & editing. Gyula Záray: Funding acquisition, Writing – review & editing.

Declaration of competing interest

The authors declare that they have no known competing financial interests or personal relationships that could have appeared to influence the work reported in this paper.

Acknowledgements

This work was supported by the National Research Development and Innovation Office of Hungary [grant number NVKP_16-1-2016-0045]. A. Demeter. acknowledges the financial support provided by the National Research Development and Innovation Office of Hungary [grant number OTKA K-128395]. The authors are grateful to Dr. Csaba Németh for performing the IR measurements, to Péter Dobosy for the ion chromatographic measurements, and to Kristóf Hegedűs for the preparation of the model compound.

Appendix A. Supplementary data

Supplementary data to this article can be found online at <https://doi.org/10.1016/j.chemosphere.2021.132393>.

References

Bolton, J.R., Bircher, K.G., Tumas, W., Tolman, C.A., 2001. Figures-of-merit for the technical development and application of advanced oxidation technologies for both electric- and solar-driven systems. *Pure Appl. Chem.* 73 (4), 627–637. <https://doi.org/10.1351/pac200173040627>.

Boulard, L., Dierkes, G., Schlüsener, M.P., Wick, A., Koschorreck, J., Ternes, T.A., 2020. Spatial distribution and temporal trends of pharmaceuticals sorbed to suspended particulate matter of German rivers. *Water Res.* 171, 115366. <https://doi.org/10.1016/j.watres.2019.115366>.

Brillas, E., 2020. A review on the photoelectro-Fenton process as efficient electrochemical advanced oxidation for wastewater remediation. *Treatment with UV*

light, sunlight, and coupling with conventional and other photo-assisted advanced technologies. *Chemosphere* 250, 126198. <https://doi.org/10.1016/j.chemosphere.2020.126198>.

- Bu, Q., Shi, X., Yu, G., Huang, J., Wang, B., Wang, J., 2016. Pay attention to non-wastewater emission pathways of pharmaceuticals into environments. *Chemosphere* 165, 515–518. <https://doi.org/10.1016/j.chemosphere.2016.09.078>.
- Comber, S., Gardner, M., Sörme, P., Leverett, D., Ellor, B., 2018. Active pharmaceutical ingredients entering the aquatic environment from wastewater treatment works: a cause for concern? *Sci. Total Environ.* 613–614, 538–547. <https://doi.org/10.1016/j.scitotenv.2017.09.101>.
- Crago, J., Bui, C., Grewal, S., Schlenk, D., 2016. Age-dependent effects in fathead minnows from the anti-diabetic drug metformin. *Gen. Comp. Endocrinol.* 232, 185–190. <https://doi.org/10.1016/j.ygcen.2015.12.030>.
- Drucker, D., Easley, C., Kirkpatrick, P., 2007. Sitagliptin. *Nat. Rev. Drug Discov.* 6 (2), 109–110. <https://doi.org/10.1038/nrd2245>.
- Duca, C., Imoberdorf, G., Mohseni, M., 2017. Effects of inorganics on the degradation of micropollutants with vacuum UV (VUV) advanced oxidation. *Journal of Environmental Science and Health, Part A* 52 (6), 524–532. <https://doi.org/10.1080/10934529.2017.1282770>.
- European Commission, 2019. European union Strategic Approach to Pharmaceuticals in the Environment: Communication from the Commission to the European Parliament, the Council and the European Economic and Social Committee. COM, p. 128, 2019. https://ec.europa.eu/environment/water/water-dangersub/pdf/strategic_approach_pharmaceuticals_env.PDF.
- Gallwitz, B., 2007. Review of sitagliptin phosphate: a novel treatment for type 2 diabetes. *Vasc. Health Risk Manag.* 3 (2), 203–210. <https://doi.org/10.2147/vhrm.2007.3.2.203>.
- Gumieniczek, A., Berecka, A., Mroczek, T., Wojtanowski, K., Dąbrowska, K., Stepień, K., 2019. Determination of chemical stability of sitagliptin by LC-UV, LC-MS and FT-IR methods. *J. Pharmaceut. Biomed. Anal.* 164, 789–807. <https://doi.org/10.1016/j.jpba.2018.11.023>.
- Gyllenhammar, I., Holm, L., Eklund, R., Berg, C., 2009. Reproductive toxicity in *Xenopus tropicalis* after developmental exposure to environmental concentrations of ethynylestradiol. *Aquat. Toxicol.* 91 (2), 171–178. <https://doi.org/10.1016/j.aquatox.2008.06.019>.
- Henning, N., Falås, P., Castronovo, S., Jewell, K.S., Bester, K., Ternes, T.A., Wick, A., 2019. Biological transformation of fexofenadine and sitagliptin by carrier-attached biomass and suspended sludge from a hybrid moving bed biofilm reactor. *Water Res.* 167, 115034. <https://doi.org/10.1016/j.watres.2019.115034>.
- Herman, G.A., Stein, P.P., Thornberry, N.A., Wagner, J.A., 2007. Dipeptidyl peptidase-4 inhibitors for the treatment of type 2 diabetes: focus on sitagliptin. *Clin. Pharmacol. Ther.* 81 (5), 761–767. <https://doi.org/10.1038/sj.cpt.6100167>.
- Hermes, N., Jewell, K.S., Falås, P., Lutze, H.V., Wick, A., Ternes, T.A., 2020. Ozonation of sitagliptin: removal kinetics and elucidation of oxidative transformation products.

- Environ. Sci. Technol. 54 (17), 10588–10598. <https://doi.org/10.1021/acs.est.0c01454>.
- Hermes, N., Jewell, K.S., Wick, A., Ternes, T.A., 2018. Quantification of more than 150 micropollutants including transformation products in aqueous samples by liquid chromatography-tandem mass spectrometry using scheduled multiple reaction monitoring. *J. Chromatogr. A* 1531, 64–73. <https://doi.org/10.1016/j.chroma.2017.11.020>.
- Ibáñez, M., Borova, V., Boix, C., Aalizadeh, R., Bade, R., Thomaidis, N.S., Hernández, F., 2017. UHPLC-QTOF MS screening of pharmaceuticals and their metabolites in treated wastewater samples from Athens. *J. Hazard Mater.* 323, 26–35. <https://doi.org/10.1016/j.jhazmat.2016.03.078>.
- Jonsson, M., Fick, J., Klaminder, J., Brodin, T., 2014. Antihistamines and aquatic insects: bioconcentration and impacts on behavior in damselfly larvae (Zygoptera). *Sci. Total Environ.* 472, 108–111. <https://doi.org/10.1016/j.scitotenv.2013.10.104>.
- Kim, H.Y., Kim, T.-H., Yu, S., 2015. Photolytic degradation of sulfamethoxazole and trimethoprim using UV-A, UV-C and vacuum-UV (VUV). *Journal of Environmental Science and Health, Part A* 50 (3), 292–300. <https://doi.org/10.1080/10934529.2015.981118>.
- Kondor, A.C., Molnár, É., Vancsik, A., Filep, T., Szeberényi, J., Szabó, L., Maász, G., Pirger, Z., Weiperth, A., Ferincz, Á., Staszny, Á., Dobosy, P., Horváthné Kiss, K., Jakab, G., Szalai, Z., 2021. Occurrence and health risk assessment of pharmaceutically active compounds in riverbank filtrated drinking water. *Journal of Water Process Engineering* 41, 102039. <https://doi.org/10.1016/j.jwpe.2021.102039>.
- Krakkó, D., Gombos, E., Licul-Kucera, V., Dóbe, S., Mihucz, V.G., Záray, G., 2019a. Enhanced photolytic and photooxidative treatments for removal of selected pharmaceutical ingredients and their degradation products in water matrices. *Microchem. J.* 150, 104136. <https://doi.org/10.1016/j.microc.2019.104136>.
- Krakkó, D., Illés, Á., Licul-Kucera, V., Dávid, B., Dobosy, P., Pogonyi, A., Demeter, A., Mihucz, V.G., Dóbe, S., Záray, G., 2021. Application of (V)UV/O₃ technology for post-treatment of biologically treated wastewater: a pilot-scale study. *Chemosphere* 275, 130080. <https://doi.org/10.1016/j.chemosphere.2021.130080>.
- Krakkó, D., Licul-Kucera, V., Záray, G., Mihucz, V.G., 2019b. Single-run ultra-high performance liquid chromatography for quantitative determination of ultra-traces of ten popular active pharmaceutical ingredients by quadrupole time-of-flight mass spectrometry after offline preconcentration by solid phase extraction from drinking and river waters as well as treated wastewater. *Microchem. J.* 148, 108–119. <https://doi.org/10.1016/j.microc.2019.04.047>.
- Kutschera, K., Börnick, H., Worch, E., 2009. Photoinitiated oxidation of geosmin and 2-methylisoborneol by irradiation with 254 nm and 185 nm UV light. *Water Res.* 43 (8), 2224–2232. <https://doi.org/10.1016/j.watres.2009.02.015>.
- Lienert, J., Bürki, T., Escher, B.I., 2007. Reducing micropollutants with source control: substance flow analysis of 212 pharmaceuticals in faeces and urine. *Water Sci. Technol.* 56 (5), 87–96. <https://doi.org/10.2166/wst.2007.560>.
- Martín, J., Buchberger, W., Santos, J.L., Alonso, E., Aparicio, I., 2012. High-performance liquid chromatography quadrupole time-of-flight mass spectrometry method for the analysis of antidiabetic drugs in aqueous environmental samples. *J. Chromatogr. B* 895–896, 94–101. <https://doi.org/10.1016/j.jchromb.2012.03.023>.
- Mathias, F.T., Fockink, D.H., Disner, G.R., Prodócimo, V., Ribas, J.L.C., Ramos, L.P., Cestari, M.M., Silva de Assis, H.C., 2018. Effects of low concentrations of ibuprofen on freshwater fish *Rhamdia quelen*. *Environ. Toxicol. Pharmacol.* 59, 105–113. <https://doi.org/10.1016/j.etap.2018.03.008>.
- Miklos, D.B., Remy, C., Jekel, M., Linden, K.G., Drewes, J.E., Hübner, U., 2018. Evaluation of advanced oxidation processes for water and wastewater treatment – a critical review. *Water Res.* 139, 118–131. <https://doi.org/10.1016/j.watres.2018.03.042>.
- OECD, 2019. *Pharmaceutical Residues in Freshwater*.
- Ramirez, A.J., Brain, R.A., Usenko, S., Mottaleb, M.A., O'Donnell, J.G., Stahl, L.L., Wathen, J.B., Snyder, B.D., Pitt, J.L., Perez-Hurtado, P., Dobbins, L.L., Brooks, B.W., Chambliss, C.K., 2009. Occurrence of pharmaceuticals and personal care products in fish: results of a national pilot study in the United States. *Environ. Toxicol. Chem.* 28 (12), 2587–2597. <https://doi.org/10.1897/08-561.1>.
- Roscher, J., Vogel, M., Karst, U., 2016. Identification of ultraviolet transformation products of diclofenac by means of liquid chromatography and mass spectrometry. *J. Chromatogr. A* 1457, 59–65. <https://doi.org/10.1016/j.chroma.2016.06.027>.
- Salim, M., El-Enany, N., Belal, F., Walash, M., Patonay, G., 2014. Micelle-enhanced spectrofluorimetric method for determination of sitagliptin and identification of potential alkaline degradation products using LC-MS. *Luminescence* 29 (1), 65–73. <https://doi.org/10.1002/bio.2503>.
- Schymanski, E.L., Jeon, J., Gulde, R., Fenner, K., Ruff, M., Singer, H.P., Hollender, J., 2014. Identifying small molecules via high resolution mass spectrometry: communicating confidence. *Environ. Sci. Technol.* 48 (4), 2097–2098. <https://doi.org/10.1021/es5002105>.
- Sonune, D., Mone, M., 2013. Isolation, characterization of degradation products of sitagliptin and development of validated stability-indicating HPLC assay method for sitagliptin API and tablets. *Int. J. Pharma Sci. Res.* 4, 3494–3503. [https://doi.org/10.13040/IJPSR.0975-8232.4\(9\).3494-03](https://doi.org/10.13040/IJPSR.0975-8232.4(9).3494-03).
- Vishnuvardhan, C., Radhakrishnanand, P., Navalgund, S.G., Satheshkumar, N., 2014. Liquid chromatography/electrospray ionisation tandem mass spectrometric study of sitagliptin and its stressed degradation products. *Drug Res.* 64 (12), 668–674. <https://doi.org/10.1055/s-0034-1370915>.
- Wardenier, N., Liu, Z., Nikiforov, A., Van Hulle, S.W.H., Leys, C., 2019. Micropollutant elimination by O₃, UV and plasma-based AOPs: an evaluation of treatment and energy costs. *Chemosphere* 234, 715–724. <https://doi.org/10.1016/j.chemosphere.2019.06.033>.
- World Health Organization, 2016. *Global Report on Diabetes*. World Health Organization, Geneva.
- Wubbels, G.G., Brown, T.R., Babcock, T.A., Johnson, K.M., 2008. The element effect and nucleophilicity in nucleophilic aromatic photosubstitution (SN₂Ar^{*}). Local atom effects as mechanistic probes of very fast reactions. *J. Org. Chem.* 73 (5), 1925–1934. <https://doi.org/10.1021/jo702468d>.
- Xia, L., Zheng, L., Zhou, J.L., 2017. Effects of ibuprofen, diclofenac and paracetamol on hatch and motor behavior in developing zebrafish (*Danio rerio*). *Chemosphere* 182, 416–425. <https://doi.org/10.1016/j.chemosphere.2017.05.054>.
- Xie, P., Yue, S., Ding, J., Wan, Y., Li, X., Ma, J., Wang, Z., 2018. Degradation of organic pollutants by Vacuum-Ultraviolet (VUV): kinetic model and efficiency. *Water Res.* 133, 69–78. <https://doi.org/10.1016/j.watres.2018.01.019>.
- Yuzbasioglu, D., Enguzel-Alperen, C., Unal, F., 2018. Investigation of in vitro genotoxic effects of an anti-diabetic drug sitagliptin. *Food Chem. Toxicol.* 112, 235–241. <https://doi.org/10.1016/j.fct.2018.01.003>.
- Zoschke, K., Börnick, H., Worch, E., 2014. Vacuum-UV radiation at 185 nm in water treatment – a review. *Water Res.* 52, 131–145. <https://doi.org/10.1016/j.watres.2013.12.034>.